Electronic Supplementary Information (ESI) for

Efficient oxygen evolution reaction catalyzed by low-density Ni-doped Co_3O_4 nanomaterials derived from metal-embedded graphitic C_3N_4

Xiaoxin Zou,[a,b] Juan Su,[c] Rafael Silva,[a,b] Anandarup Goswami,[a,b] Bhaskar R. Sathe,[a,b] and Tewodros Asefa[a,b]*

[a] Department of Chemistry and Chemical Biology, Rutgers, The State University of New Jersey, 610 Taylor Road, Piscataway, New Jersey 08854, USA

[b] Department of Chemical and Biochemical Engineering, Rutgers, The State University of New Jersey, 98 Brett Road, Piscataway, New Jersey 08854, USA

[c] State Key Laboratory of Inorganic Synthesis and Preparative Chemistry, Jilin University, Changchun 130012, China.

* E-mail: tasefa@rci.rutgers.edu

Experimental Section

Chemicals and Reagents: Nickel(II) chloride hexahydrate, cobalt(II) chloride hexahydrate, dicyandiamide, citric acid and ethylene glycol were purchased from Sigma-Aldrich. All the reagents were of analytical grade and used as received without further purification. Deionized water was used throughout the experiments.

Preparation of Ni-doped Co_3O_4 nanonetworks (Ni-Co_3O_4-A) *via* Route A: In Route A, the Ni-Co_3O_4-A catalysts were synthesized from *crystalline* g-C_3N_4-based polymer that contained different mole ratios of Ni(II) and Co(II) ions. In a typical synthesis of Ni-Co_3O_4-A with Ni:Co atomic ratio = 1:9, dicyandiamide (12 mmol) was uniformly mixed with nickel(II) chloride hexahydrate ($NiCl_2{\cdot}6H_2O$, 0.04 mmol) and cobalt(II) chloride hexahydrate ($CoCl_2{\cdot}6H_2O$, 0.38 mmol). The mixture was then heated at 500 °C in a tube furnace for 3 h under N_2 atmosphere. After cooling to room temperature, the final solid product (metal ions-containing g-C_3N_4) was collected without further purification. The metal ion-containing g-C_3N_4 was then calcined in air at 450 °C to produce a black powder, which was denoted as Ni-Co_3O_4-A. By varying the ratio of $NiCl_2{\cdot}6H_2O$ to $CoCl_2{\cdot}6H_2O$ but keeping the dicyandiamide and the rest of reaction procedures the same, various Ni-doped Co_3O_4 samples with different Ni:Co ratios were obtained. The quantitative elemental analysis by inductively coupled plasma mass spectrometry (ICP-MS) indicated that the Ni:Co atomic ratios in the as-prepared materials were very close to the nominal values of the metal sources used.

Preparation of Ni-doped Co_3O_4 samples (Ni-Co_3O_4-B) *via* Route B: For comparative purpose, a second synthetic route (Route B) involving a classic *amorphous* polymer-metal complex synthetic route as described previously[S1] was also used for preparation of Ni-doped Co_3O_4 samples. This route, Route B, was based on a metal ion-containing polyester network, which was formed by the polyesterification reaction between citric acid and ethylene glycol.[S1] In a typical synthesis, nickel(II) chloride hexahydrate ($NiCl_2{\cdot}6H_2O$, 0.04 mmol), cobalt(II) chloride hexahydrate ($CoCl_2{\cdot}6H_2O$, 0.38 mmol), ethylene glycol (43 mmol), and anhydrous citric acid (28 mmol) were added to methanol (15 mL) with stirring for 5 h at room temperature. The as-obtained transparent solution was heated to 130 °C to promote esterification between ethylene glycol and citric acid, yielding a glassy resin. Then, the metal ions-containing resin was calcined in air at 450 °C to produce a black powder, denoted as Ni-Co_3O_4-B. The quantitative elemental analysis by ICP-MS indicated that the Ni:Co atomic ratios in the as-prepared materials were very close to the nominal values of the metal sources used during the synthesis.

General Characterization: The powder X-ray diffraction (XRD) patterns were recorded on a Rigaku D/Max 2550 X-ray diffractometer with Cu Kα radiation (λ = 1.5418 Å). The scanning electron microscopic (SEM) images were taken on a JEOL JSM 6700F electron microscope. The TEM images were obtained with a Topcon

002B TEM microscope, whereas the HRTEM image was obtained with a JEOL JSM-3010 TEM microscope. The X-ray photoelectron spectroscopy (XPS) was performed on an ESCALAB 250 X-ray photoelectron spectrometer with a monochromatized X-ray source (Al Kα *hv* = 1486.6 eV). The energy scale of the spectrometer was calibrated using Au $4f_{7/2}$, Cu $2p_{3/2}$, and Ag $3d_{5/2}$ peak positions. The standard deviation for the binding energy (BE) values is 0.1 eV. The UV-Vis diffuse reflectance spectra were recorded on a Lambda 950 spectrophotometer (PerkinElmer). The nitrogen adsorption and desorption isotherms were measured using a Micromeritics ASAP 2020M system. Owing to the fact that the samples are extremely light weight and fluffy, getting their masses precisely and getting the samples in similarly untapped state and under the same conditions was proven to be difficult; this has caused some inherent fluctuations on the surface area values we obtained (please note that a very slight change on the mass and the degree of tapping of such types of samples can cause significant changes in the value of surface area per mass of the materials, especially when the surface areas of the materials are not so high as do in our case). Therefore, the BET surface areas were of each sample is measured five times each, and the average BET surface areas and the corresponding standard deviations have been provided in the revised manuscript. The ICP elemental analyses were performed on a Perkin-Elmer Optima 3300DV ICP spectrometer. The solid-state ^{13}C (100.64 MHz) NMR spectra were acquired on a Brüker 400 MHz NMR spectrometer consisting of a 3.2 mm HXY Brüker probe operating in HX mode at 298K. For ^{13}C CP-MAS NMR experiments, 10.0 kHz spin rate, 3 s recycle delay, 2 ms contact time, $\pi/2$ pulse width of 5 μs (at 66 W) and at least 16 K scans using “Spinal 64” ^{1}H decoupling method were employed. The ^{13}C chemical shift was referenced using adamantine as external standard. The spectra were processed in Brüker Topspin (*v* 3.1) using conventional techniques and 50 Hz of line broadening window function was applied to all the spectra.

Electrochemical measurements: The electrocatalytic properties of the materials were studied with a three-electrode system using a PAR Versastat3 (Princeton Applied Research) instrument. A saturated calomel electrode (SCE) and a platinum wire (diameter: 0.25 mm) were used as the reference electrode and as the counter electrode, respectively. To prepare the working electrode, 2 mg of catalyst and 20 μL 5 wt. % Nafion were dispersed in ethanol (180 μL) under sonication for at least 30 min to form a homogeneous mixture. Then, 1 μL of this solution was drop-casted onto a 3 mm in diameter glassy carbon electrode (GCE), and it was left to dry in air. This gave a catalyst loading of ~0.14 mg/cm^2 on the GCE. By using this electrode as the working electrode, electrochemical measurements of the samples with a scan rate of 50 mV/s were measured in 0.1 M NaOH solution, which was used as electrolyte. Please note that the Ni-Co_3O_4-A material retained its porous structure even after being mixed with Nafion (see Fig. S12 in ESI).

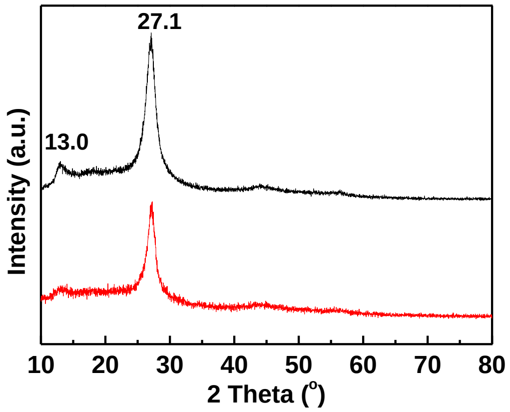

Fig. S1. XRD patterns of pure g-C_3N_4 (black line) and Ni, Co ions-doped g-C_3N_4 (with Ni:Co = 1:9) (red line) that was used as precursor for Ni-Co_3O_4 sample.

For pure g-C_3N_4, the strong peak at 27.1° (2-theta) was indexed as the stacking of (002) planes of g-C_3N_4, whereas the weak peak at 13.0° (2-theta) was attributed to the in-plane repeat units of heptazines in the g-C_3N_4. The XRD patterns of Ni, Co ions-containing g-C_3N_4 was found to be similar to the XRD pattern of pure g-C_3N_4, except for a slight decrease in the intensity of the diffraction peaks, especially the one at 13.0° (2-theta). This result indicates that the two materials have similar structures, or the structural features of g-C_3N_4 remain unchanged upon doping with nickel and cobalt ions. Moreover, compared with the XRD pattern of pure g-C_3N_4, the Ni, Co ions-doped g-C_3N_4 sample did not exhibit any new diffraction peak(s) associated with impurities (*e.g.*, metal chloride, metal oxides, metal nitrides, or metal carbides). This result also indicates that the metal ions in the Ni, Co ions-containing g-C_3N_4 sample are most likely present only as chemically immobilized species within the in-plane cavities of g-C_3N_4 host by coordinating with the electron-donating N-based ligands, as observed in metal-based porphyrine systems.[S2] These conclusions are also in line with those reported by Wang et al. for Fe^{3+}(Zn^{2+})-doped g-C_3N_4.[S3]

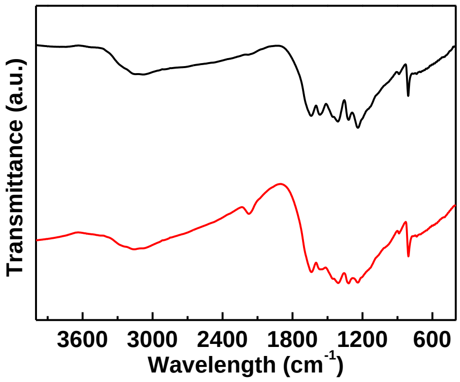

Fig. S2. FT-IR spectra of pure g-C_3N_4 (black line) and the Ni- and Co ion-doped g-C_3N_4 sample, with Ni:Co = 1:9 (red line).

Fig. S2 shows the FT-IR spectra of pure g-C_3N_4 and the Ni, Co ions-doped g-C_3N_4 sample. The spectra depict well-resolved and strong IR absorption bands, which are related to the typical molecular structure of g-C_3N_4. The intense, broad IR band ranging from 1232 to 1671 cm^{-1} is assigned to the typical stretching vibration modes of heptazine units. The other intense IR band at 810 cm^{-1} is attributable to the out-of-plane bending vibration of the same heptazine units. Although the two IR spectra appear very similar, small differences can actually be seen upon careful examination of the spectra and by comparing the spectrum of the metal ions-doped g-C_3N_4 sample with that of g-C_3N_4. This includes the appearance of a new weak absorption band at *ca*. 2176 cm^{-1} and the weakening of the hyperfine absorption bands related to heptazine units in the metal ions-containing g-C_3N_4. The new weak absorption band at *ca*. 2176 cm^{-1} was assigned to the stretching mode of carbon-nitrogen (C≡N) triple bond. The presence of C≡N bonds in the materials is not unexpected considering the fact that C≡N bonds sometimes form as defect sites within g-C_3N_4 materials.[S4] Therefore, our result here further suggests that the doping metal ions in g-C_3N_4 promotes the formation of C≡N defect sites in the latter. In addition, the weakening of the absorption bands associated with heptazine units in the metal ions-doped g-C_3N_4 sample demonstrates that the metal ions must be chemical attached to the heptazine units through coordination bonds. Considering the fact that the incorporation of dopants in a host material almost always leads to some inherent changes in the local microstructure and the composition of the host material, these IR results indicating some structural changes in the Ni, Co ions-doped g-C_3N_4 sample are not unprecedented.

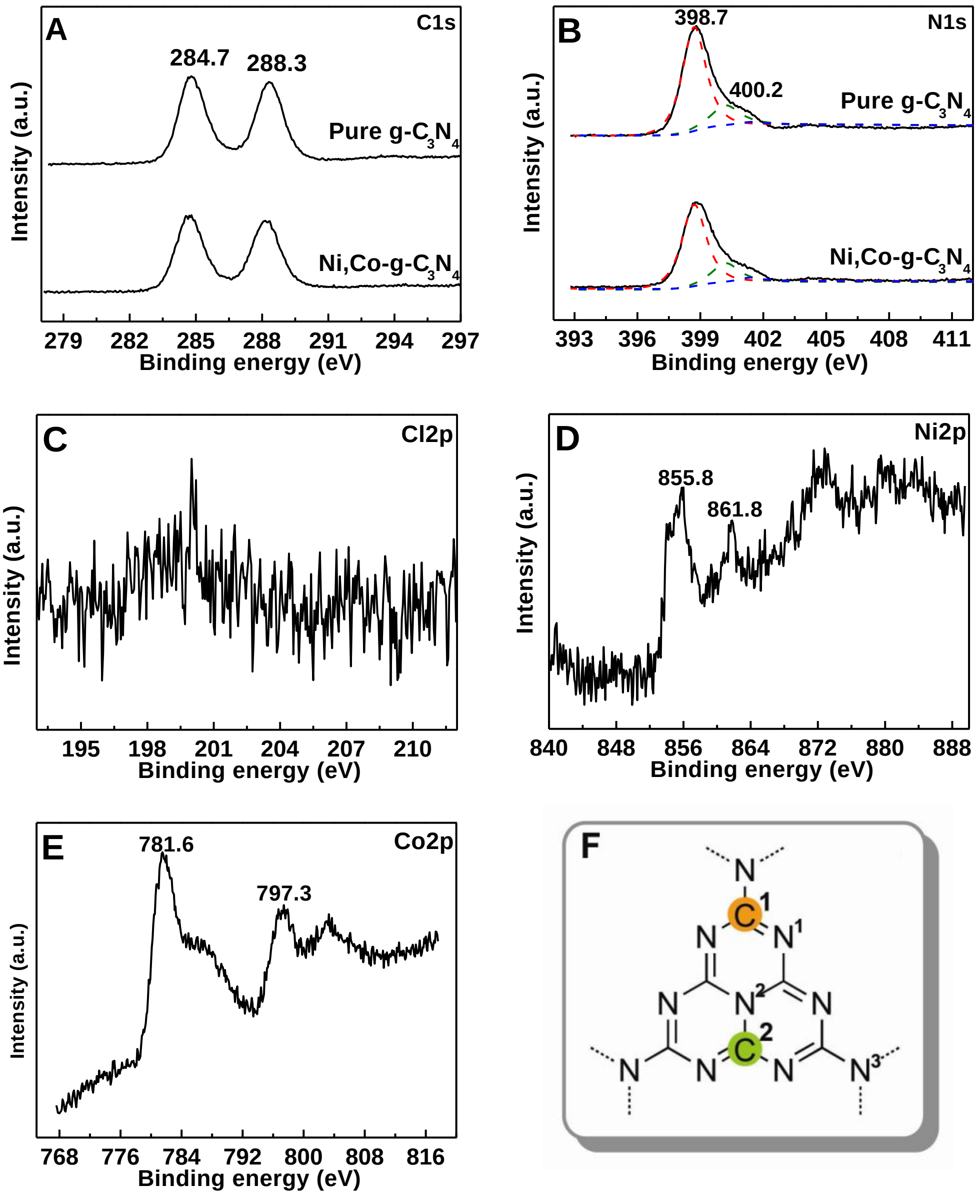

Fig. S3. (A) C1s, (B) N1s, (C) Cl2p, (D) Ni2p and (E) Co2p XPS spectra of the Ni, Co ions-containing g-C_3N_4 sample (Ni:Co = 1:9). For comparison, C1s and N1s XPS spectra of pure g-C_3N_4 were also included in Fig. S3A,B. (F) the basic structural unit of g-C_3N_4.

X-ray photoelectron spectroscopy (XPS) was performed to further obtain information about the composition of the Ni, Co ions-doped g-C_3N_4 sample. For comparison, C1s and N1s XPS spectra of pure g-C_3N_4 were also measured. The XPS spectra associated with C1s of the two samples (Fig. S3,A) exhibit two similar peaks: the first at *ca*. 284.7 and the second at *ca*. 288.3 eV. The peak at *ca*. 284.7 eV is due to adventitious elemental carbon from the XPS instrument itself.[S5] The peak at *ca*.

288.3 eV, however, corresponds to $\underline{C}$-$(N)_3$ carbon atoms (both C1 and C2 type carbon species in Fig. 2,F) of g-C_3N_4.[S6]

The XPS spectra of N1s of the two samples are shown in Fig. S3,B. The N1s peak was deconvoluted into two components with two discernible binding energies: at 398.7 and 400.2 eV, which were ascribed to the nitrogen atoms in $\underline{N}$-C_2 (N1's in Fig. S3,F) and $\underline{N}$-C_3 (both N2's and N3's in Fig. S3,F) modes, respectively.[S6] The quantitative analysis of the XPS data revealed that the N1/(N2 + N3) atomic ratio was ~1.00:0.28 for all the two samples, which is very close to theoretical value of 1:0.33 (considering the contribution of different nitrogen atoms in unit cell of g-C_3N_4), and also confirms the successful synthesis of carbon nitride skeleton. The similarity in the XPS spectra associated with C1s and N1s (Figs. S3,A and B) of the two samples and their similar values of N1/(N2 + N3) corroborate the conclusion made above that the bulk structure of g-C_3N_4 remains unchanged after doping with metal ions (nickel and cobalt ions). Although C≡N species were observed on the IR spectra of M-C_3N_4, they were difficult to deconvolute from the N1s XPS spectrum. This is because (1) the amount of C≡N bonds in M-C_3N_4 should be very low, as indicated by the very weak IR absorption of C≡N bonds in IR spectrum and (2) C≡N groups have low sensitivity on XPS, and they are therefore often hard to elucidate; this difficulty was also encountered by others in previously works as well.[S4c-g]

The XPS analysis also allowed us to determine the Cl^- content in the Ni, Co ions-doped g-C_3N_4 sample. Fig. S3C shows a very weak Cl2p signal, indicating that the Cl^- content in the sample is very small. This was confirmed by elemental analysis, which indicated the Cl/metal atomic ratio to be very small (0.04) in this sample. This value is obviously much lower than the Cl/metal ion atomic ratio of 2:1 in the metal precursors used ($NiCl_2\cdot 6H_2O$ and $CoCl_2\cdot 6H_2O$). Nonetheless, the result is consistent with that previously reported for Fe^{3+}-doped g-C_3N_4, which was synthesized by using $FeCl_3$ as the iron source and which also showed a very low Cl/Fe molar ratio.[S3] This result confirms further that metal ions in this sample are mainly coordinated with the g-C_3N_4 host via coordination bond with the N-atoms of g-C_3N_4, rather than with $Cl^–$ ions.

Figs. S3,D and S3,E show the XPS spectra of Ni2p and Co2p in the Ni, Co ions-doped g-C_3N_4 sample. In Fig. S3,D, the spectra exhibit the binding energies of Ni2$p_{3/2}$ peak and a satellite peak at 855.8 and 961.8 eV, respectively. This demonstrates that Ni species in the sample are divalent (Ni^{2+}).[S7] The Co2p XPS spectrum (Fig. S3E) exhibits the binding energies of Co2$p_{3/2}$ and Co2$p_{1/2}$ at 781.6 and 797.3 eV, respectively. The distance of the two peaks is *ca*. 15.7 eV, which is in agreement with a previously reported value for Co^{2+}.[S8] In addition, the intense satellite peaks observed at the high binding-energy side of the main peaks also demonstrate that cobalt ions are present in form of Co^{2+}.

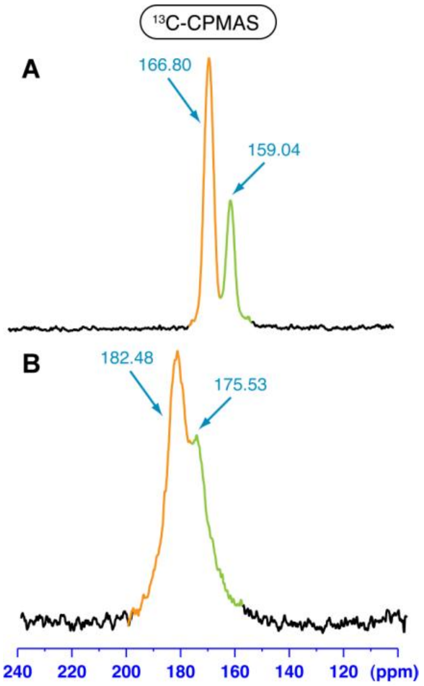

Fig. S4. Solid-state ^{13}C CP-MAS spectra of (A) pure C_3N_4 and (B) M-C_3N_4.

In order to further confirm that the metal ions were embedded in the framework of g-C_3N_4, ^{13}C cross-polarization MAS solid-state NMR (^{13}C CP-MAS) spectra were recorded for the g-C_3N_4 samples before and after metal-doping. It should be pointed out that the ^{13}C CP-MAS spectra can offer some important qualitative information regarding the different types of carbon species present in the material.[S9] The pure g-C_3N_4 sample showed two peaks, the first at 166.80 ppm (marked in orange) and the second at 159.04 ppm (marked in green). These chemical shifts correspond to different carbons of heptazines and are in accordance with the chemical shift values previously reported for different compounds containing heptazine units.[S9] The peak at 166.80 ppm corresponds to the group of carbon atoms connected in a $\underline{C}\{(N^1)_2\}\{(N^3)_1\}$ fashion (C1's in Fig. S3C), whereas the peak at 159.04 ppm is associated with the group of carbon atoms attached in a $\underline{C}\{(N^1)_2\}\{(N^2)_1\}$ mode (C2's in Fig. S3F). In comparison with the spectrum of pure g-C_3N_4 (Fig. S4A), the NMR spectrum of M-C_3N_4 exhibited very large differences in chemical shifts. For example, the peak associated with C1's showed up at 166.80 ppm for pure g-C_3N_4, but the peak shifted to 182.48 ppm in M-C_3N_4. Similarly, the peak corresponding to C2's appeared at 159.04 ppm for pure g-C_3N_4, but moved to 175.53 ppm in case of M-C_3N_4. Considering that the metal ions are not directly connected to the carbon atoms of g-C_3N_4 but rather to the nitrogen atoms, these quite significant peak shifts on the ^{13}C CP-MAS NMR spectra demonstrate that the metal species are likely to be chemically bound with the g-C_3N_4 crystal structure, rather than physically mixed with it.

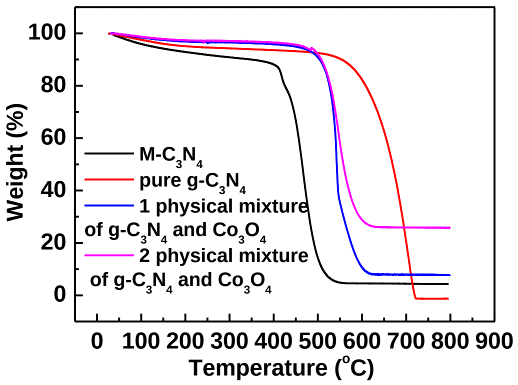

Fig. S5. Thermogravimetric (TG) curves obtained by heating pure $g-C_3N_4$ (red line), $M-C_3N_4$ (black line) and two physical mixtures of $g-C_3N_4$ and Co_3O_4 in different ratios (blue and pink lines) in air.

The thermogravimetric (TG) analysis of pure $g-C_3N_4$ and $M-C_3N_4$ sample was carried out in air from 25 to 800 °C, and the results are shown in Fig. S4. The pure C_3N_4 was observed to be very stable till 540 °C in air, but it then started to loss weight from ~540-720 °C. By contrast, the thermal decomposition temperature of $M-C_3N_4$ began at significantly lower temperature of 400 °C. For comparison, two physical mixtures of Co_3O_4 and $g-C_3N_4$ with sample ratios of 10:100 and 30:100 were measured under the same condition. It is seen that the physically-mixed Co_3O_4 also decreased the decomposition temperature of $g-C_3N_4$ to a certain extent. However, the decomposition temperature of the physical mixtures of Co_3O_4 and $g-C_3N_4$ was still much higher than that of $M-C_3N_4$. These results further unequivocally demonstrate that metal ions must be chemically incorporated into the $g-C_3N_4$ crystal structure, rather than physically mixed with $g-C_3N_4$. This also indicates that although metal doping does not change the core chemical skeleton of $g-C_3N_4$ much (as seen in XRD patterns), it appears to have a strong influence on the nature of chemical bonds of $g-C_3N_4$, and thus its thermal stability. Furthermore, from the amount of inorganic residue (metal oxides) left after the thermal decomposition of $Ni,Co-C_3N_4$, the empirical compositions of the sample was deduced to be $0.006Ni \cdot 0.056Co \cdot C_3N_4$.

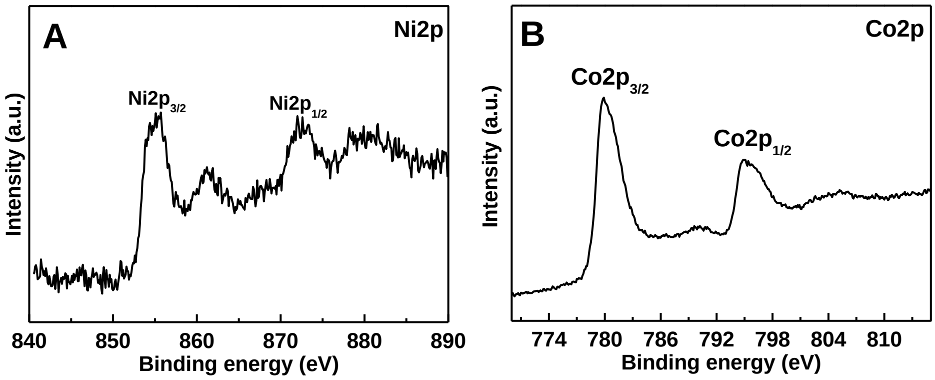

Fig. S6. (A) Ni2p and (B) Co2p XPS spectra for Ni-Co_3O_4-A.

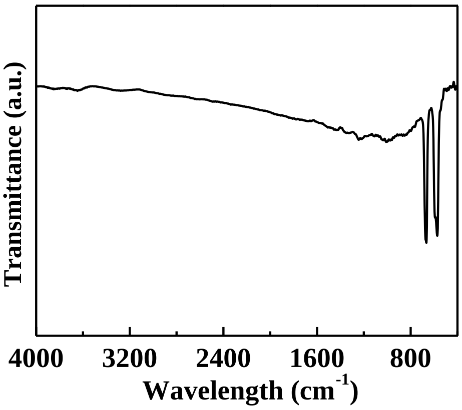

Fig. S7. IR spectrum of Ni-Co_3O_4-A.

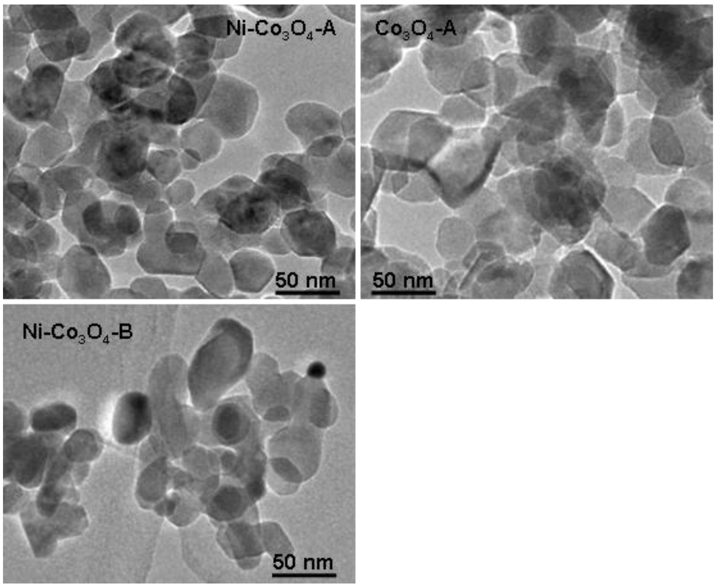

Fig. S8. TEM images of Ni-Co_3O_4-A, Co_3O_4-A and Ni-Co_3O_4-B.

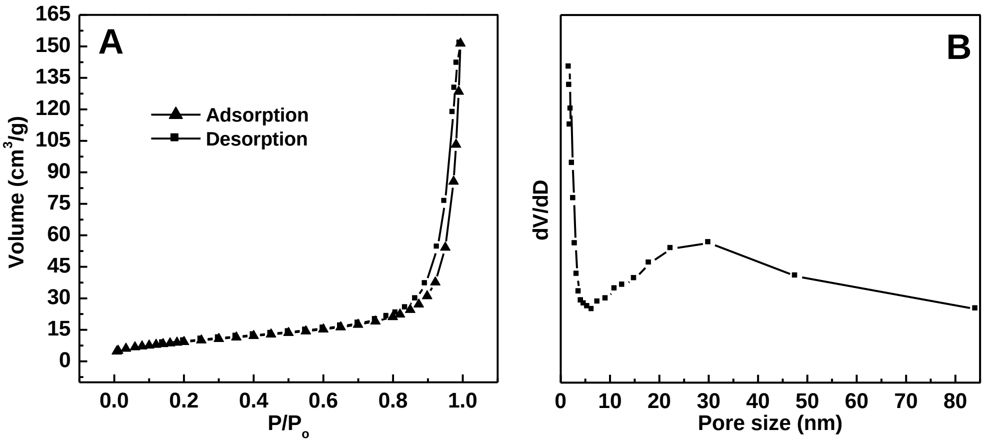

Fig. S9. (A) N_2 adsorption-desorption isotherms and (B) the corresponding BJH pore size distribution of Ni-Co_3O_4-A.

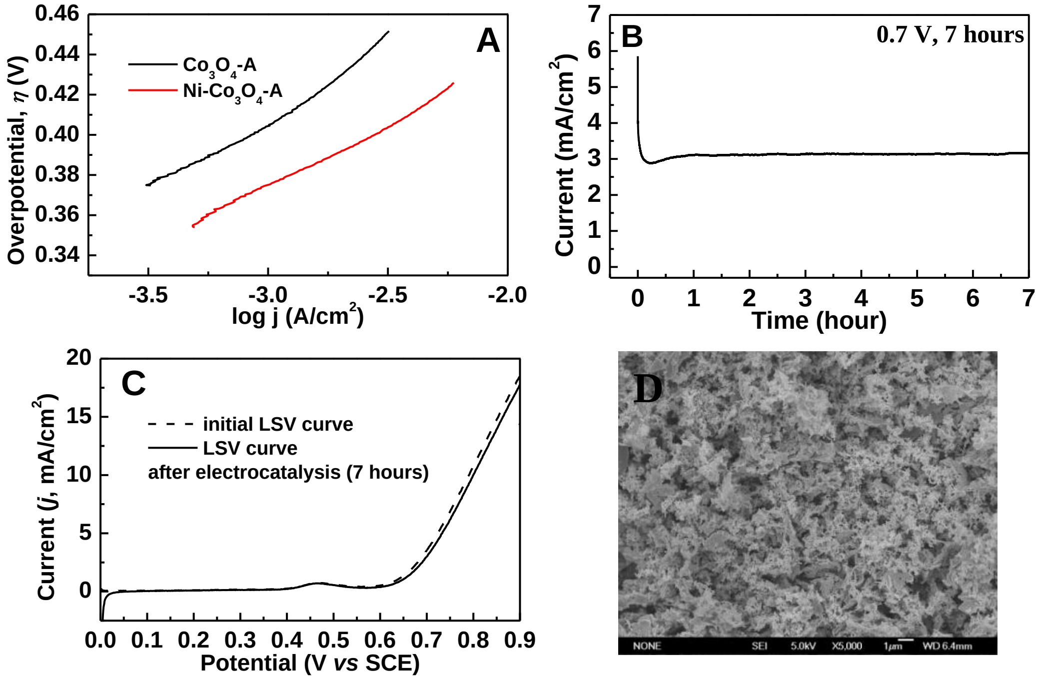

Fig. S10. (A) The Tafel plots obtained in 0.1 M KOH for Co_3O_4-A and Ni-Co_3O_4-A. The Tafel slopes were about 75 and 62 mV dec^{-1} for Co_3O_4-A and Ni-Co_3O_4-A, respectively. The exchange current densities were about 2.8 x 10^{-8} and 4 x 10^{-8} A cm^{-2} mg^{-1}, respectively. It should be pointed out that the exchange current density of Ni-Co_3O_4-A is larger than those of the previously-reported Ni-doped Co_3O_4 samples (2.6 x 10^{-9} A cm^{-2} mg^{-1} for reference S10a and 1.4 x 10^{-8} A cm^{-2} mg^{-1} for reference S10b. This demonstrates that our Ni-doped Co_3O_4 nanomaterialis a highly active water oxidation electrocatalyst. (B) A current-time (I-t) graph obtained for an oxygen evolution reaction in the presence of Ni-Co_3O_4-A at -0.7 V. (C) Typical LSV curves before and after I-t measurement in the presence of Ni-Co_3O_4-A. (D) the SEM image of Ni-Co_3O_4-A after I-t measurement. The sample loading on the glassy carbon electrode (the working electrode) was 0.14 mg/cm^2.

FT-IR Measurements. First, in a dry glove box, the dry solid sample was closely filled and sealed in an IR cell with two CaF_2 windows (25 mm in diameter and 3 mm in thickness). Subsequently, when the FT-IR spectrum of the dry solid sample was obtained, H_2O vapor was injected into the IR cell, which was maintained in H_2O vapor for 10 min. After removing the excess water by vacuum drying process, the IR spectrum of the sample was measured again.

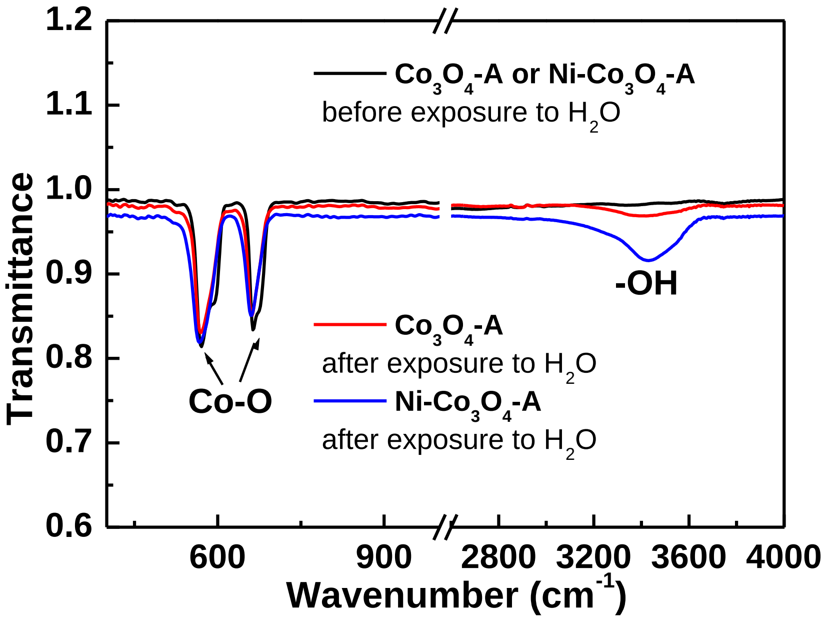

Fig. S11. FT-IR spectra of Co_3O_4-A and Ni-Co_3O_4-A before and after exposure to H_2O vapor (the operation details are presented below). As shown in Fig. S10, a broad IR band with maximum at about 3430 cm^{-1} appears for the Co_3O_4-A and Ni-Co_3O_4-A samples after exposure to H_2O, and this band corresponds to H-bonded OH stretching vibrations. Obviously, Ni-Co_3O_4-A exhibits a stronger OH absorption band than Co_3O_4-A, indicating that Ni-Co_3O_4-A possesses a stronger adsorption ability of water molecules than Co_3O_4-A. The OH absorption intensity was normalized based on the Co-O absorptions. It is worth noting here that previously reported works also showed that nickel oxide or hydroxide had the ability to improve the absorption/dissociation of water of related materials in electrocatalytic hydrogen evolution reaction as well (see reference S11 in ESI).[S11]

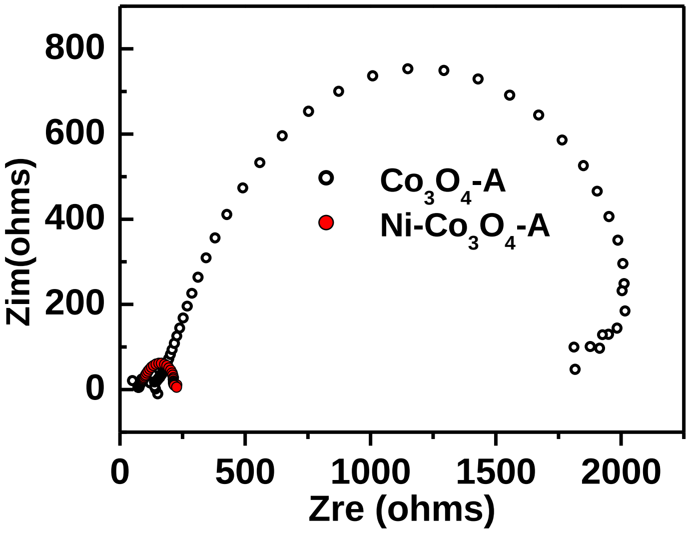

Fig. S12. Electrochemical impedance plots obtained at a potential of 0.62 V for Co_3O_4-A (black) and Ni-Co_3O_4-A (red). From the figure, it is seen that Ni-Co_3O_4-A exhibits much smaller Faradaic impedance (or charge-transfer impedance) than Co_3O_4-A, indicating the markedly faster OER kinetics with Ni-Co_3O_4-A.[S12]

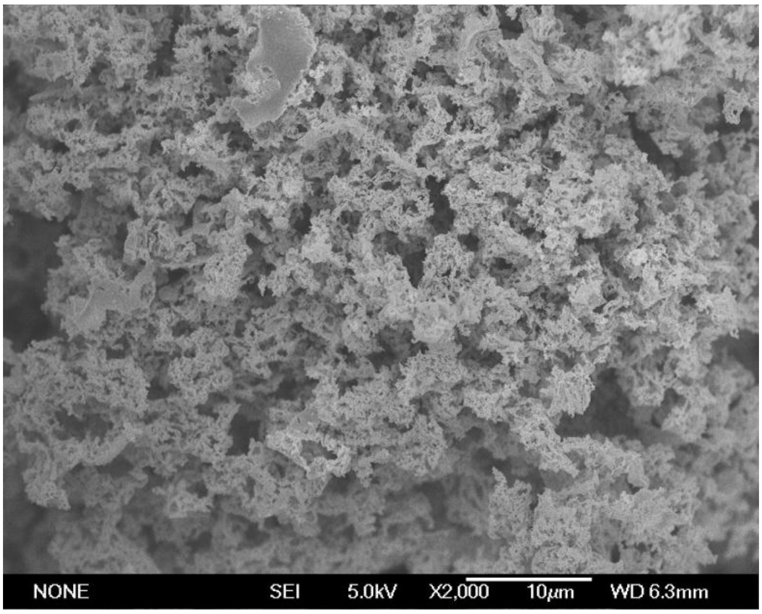

Fig. S13. The SEM image of Nafion-impregnated Ni-Co_3O_4-A sample. The image shows that that Ni-Co_3O_4-A retains its porous structure even after being mixed with Nafion.

Supporting Information References

S1. M. Kakihana, and M. Yoshimura, *Bull. Chem. Soc. Jpn.*, 1999, **72**, 1427; M. P. Pechini, U.S. Patent 330697, 1967.

S2. B. Su, I. Hatay, A. Trojánek, Z. Samec, T. Khoury, C. P. Gros, J.-M. Barbe, A. Daina, P.-A. Carrupt, H. H. Girault, *J. Am. Chem. Soc.* 2010, **132**, 2655.

S3. X. Wang, X. Chen, A. Thomas, X. Fu, and M. Antonietti, *Adv. Mater.*, 2009, **21**, 1609.

S4. a) T. Komatsu, T. Nakamura, *J. Mater. Chem.* 2001, **11**, 474; b) D. R. Miller, J. R. Holst, E. G. Gillan, *Inorg. Chem.* 2007, **46**, 2767; c) S. M. Lyth, Y. Nabae, S. Moriya, S. Kuroki, M. Kakimoto, J. Ozaki, S. Miyata, *J. Phys. Chem. C* 2009, **113**, 20148; d) Q. Liu, J. Zhang, *Langmuir* 2013, **29**, 3821; e) G. Li, N. Yang, W. Wang, W. F. Zhang, *J. Phys. Chem. C* 2009, **113**, 14829; f) D. R. Miller, J. Wang, E. G. Gillan, *J. Mater. Chem.* 2002, **12**, 2463; g) J. Su, X.-X. Zou, Y.-C. Zou, G.-D. Li, P.-P. Wang, J.-S. Chen, *Inorg. Chem.* dx.doi.org/10.1021/ic400109j.

S5. a) J. Su, X.-X. Zou, G.-D. Li, X. Wei, C. Yan, Y.-N. Wang, J. Zhao, L.-J. Zhou,and J.-S. Chen, *J. Phys. Chem. C*, 2011, **115**, 8064; b) X. Zou, J. Liu, J. Su, F. Zuo, J. Chen and P. Feng, *Chem. Eur. J.*, 2013, **19**, 2866.

S6. X.-X. Zou, G.-D. Li, Y.-N. Wang, J. Zhao, C. Yan, M.-Y. Guo, L. Li and J.-S. Chen, *Chem. Commun.*, 2011, **47**, 1066.

S7. A. P. Grosvenor, M. C. Biesinger, R. S. C. Smart, N. S. McIntyre, *Surf. Sci.*, 2006, **600**, 1771.

S8. J. G. Dillard, C. V. Schenck, and M. H. Koppelman, *Clays Clay Miner.*, 1983, **31**, 69.

S9. a) B. Jürgens, E. Irran, J. Senker, P. Kroll, H. Müller, W. Schnick, *J. Am. Chem. Soc.* 2003, **125**, 10288; b) J. R. Holst, E. G. Gillan, *J. Am. Chem. Soc.* 2008, **130**, 7373; c) J. Zhang, G. Zhang, X. Chen, S. Lin, L. Möhlmann, G. Dołęga, G. Lipner, M. Antonietti, S. Blechert, X. Wang, *Angew. Chem. Int. Ed.* 2012, **51**, 3183.

S10. a) Y. Li, P. Hasin, Y. Wu, *Adv. Mater.*, 2010, **22**, 1926; b) B. Lu, D. Cao, P. Wang, G. Wang, Y. Gao, *Int. J. Hydrogen Energy*, 2011, **36**, 72.

S11. R. Subbaraman, D. Tripkovic, D. Strmcnik, K.-C. Chang, M. Uchimura, A. P. Paulikas, V. Stamenkovic, N. M. Markovic, *Science*, 2011, **334**, 1256; and references therein.

S12. G. Wu, N. Li, D.-R. Zhou, K. Mitsuo, B.-Q. Xu, *J. Solid State Chem.*, 2004, **177**, 3682.